

# EVLA Memo #49

## Attenuation of Radio Frequency Interference by Interferometric Fringe Rotation

Rick Perley

November 15, 2002

### Abstract

It is shown that the VLA, as an imaging interferometer, attenuates unwanted signals by a factor of from 14 to 50 dB compared to a total-power telescope of the same sensitivity. The unwanted emissions standards for equipment located at the EVLA site can therefore be relaxed by  $\sim 15$  dB over those based on standards established for a total power system. A simple expression is given which allows estimation of the approximate attenuation arising from fringe rotation as a function of frequency, array scale, interference duration, and target source declination.

## 1 Introduction

Modern radio telescopes are exquisitely sensitive, and hence extremely vulnerable to unwanted emissions which enter through the telescope sidelobes. The effects of unwanted emissions on a total-power system can be estimated in a straightforward manner, the results of which have led to the well-known ITU standards on harmful emissions. The effects of external signals on multi-element, imaging interferometers are more difficult to calculate due to the effects of differential phase between the target source and the source of unwanted emissions.

In this memo, I review the basics of attenuation of unwanted signals for both total-power and interferometric systems. An analysis based on the imaging response gives attenuation estimates which are in excellent agreement with the analysis of Thompson[2]. The predicted attenuation is compared to those generated by simulations, and a ‘universal attenuation relationship’ is proposed, which allows easy and fairly accurate estimates of the attenuation of RFI due to the interferometric imaging process.

## 2 RFI and a Total Power Antenna

The analysis of the effect of RFI on a total power radio astronomy system is straightforward. A source of radio frequency interference with power flux density  $F_h$ , entering through a sidelobe of gain  $G_{sl}$  is considered to be harmful to a radio astronomical observation if the power detected within a bandwidth  $\Delta\nu$  exceeds 10% of the power from the astronomical source within that same bandwidth. If one observes an astronomical source with spectral power flux density  $S_{obj}$  with an antenna of forward gain  $G$  (defined with respect to isotropic), and a receiver bandwidth  $\Delta\nu$ , this harmful condition can be expressed as

$$F_h < \frac{S_{obj}}{20} \frac{G}{G_{sl}} \Delta\nu \quad (1)$$

where the extra factor of one-half is due to an assumption that the source is unpolarized. The standard expression for harmful threshold power flux density can then be derived by noting that the relevant source spectral flux density is normally taken to be the minimum detectable spectral power flux density, given by

$$S_{min} = \frac{8\pi k T_{sys}}{G \lambda^2 \sqrt{\Delta\nu}} \quad (2)$$

from which one obtains

$$F_h < \frac{0.4\pi k T_{sys}}{G_s \lambda^2} \sqrt{\frac{\Delta\nu}{\tau}} \quad (3)$$

This power flux density can be related to the transmitter power,  $P_t$  through the equation

$$F_h = \frac{SP_t G_t}{4\pi r^2} \quad (4)$$

where  $r$  is the distance from the transmitter to the astronomical antenna,  $G_t$  is the gain of the transmitting antenna in the direction of the astronomical antenna, and  $S$  represents the effects of shielding lying between the transmitter and receiver.

These relationships have been used to establish the maximum emission standards for equipment located at the VLA site[1].

### 3 RFI and a Single-Baseline Interferometer

The expansion of the total-power result to a single-baseline interferometer is straightforward if we ignore the effects of differential source motion – that is, if we consider an interferometer on a non-rotating platform. For this, an analysis gives the same result as for the total-power case, except that the coefficient is reduced by  $\sqrt{2}$ , (because we assume two antennas of forward gain equal to that assumed in the total-power case) and all variables are replaced by the geometric means of the two antennas – for example, the mean sidelobe gain is  $\sqrt{G_{s1}G_{s2}}$ , and the mean distance is  $r = \sqrt{r_1 r_2}$ . However, all practical interferometers are built on rotating platforms (the most obvious example being the earth), and a proper analysis must consider the effects of differential motion between the target source and interfering source.

Imaging interferometers measure the complex coherence of the emission, with phase and delay tracking inserted so that the observed complex coherence will be constant for an unresolved object at the phase and delay tracking center. When referenced to the phase tracking center, emission from another direction undergoes a phase rotation at a rate given by:

$$\nu_F = \omega_e (u_0 \cos \delta_0 - u \cos \delta) \quad (5)$$

where  $u = B_x \cos H + B_y \sin H$  is the projected E-W component of the interferometer baseline, measured in wavelengths,  $\omega_e$  is the angular rotation rate of the earth, and the subscripts refer to the phase tracking source.<sup>1</sup>

Interference rarely enters the telescope through the primary beam (and the effects are potentially very harmful if it does!). More commonly, it enters through some sidelobe or sidelobes, so that the amplitude and phase of the emission – and hence the amplitude and phase of the correlator response to RFI – are modified by the antenna’s sidelobe radiation characteristics. These sidelobes have characteristic size  $\theta \sim \lambda/D$ , and thus impose a characteristic time  $t \sim \lambda/\omega_e D$  seconds for significant changes in the phase and amplitude of the correlated response. For the VLA, this timescale is  $\sim 165/\nu_G$  seconds, where  $\nu_G$  is the frequency in GHz.

The interferometer phase response to RFI is also a function of the interferor’s motion with respect to the phase tracking center. If the interferor is stationary, then the correlator phase is simply that of the fringe-tracking system, and the RFI is equivalent to that from an object at the north pole, but with its phase and amplitude modified by the appropriate sidelobe gains. This phase rate is considerably faster than that imposed by the motion of the stationary source through the antenna sidelobe pattern.

Thus, for the purposes of calculating the effects of stationary RFI on synthesis imaging, we can replace the real interfering source with a north pole equivalent, noting that the amplitudes and phases have imposed on them a slowly varying offset given by the difference between the antennas’ sidelobe patterns for the true interfering source’s direction.

For a stationary emitter, the phase frequency in a phase-tracking interferometer is obtained from Eq. 5 by setting  $\cos \delta_0 = 90$ , giving

$$\nu_f = -\omega_e u \cos \delta \quad (6)$$

We now imagine observing a natural source of emission at declination  $\delta$ , added to which is a source of stationary RFI which has the same phase rate as a source at the north pole. In the simplest analysis, the complex visibility is vectorially summed over some period of time,  $t$ . The desired signal adds coherently, since its natural phase rate has been offset by the phase-tracking system, while the interferor adds incoherently, as its phase is cycling at the natural rate. After time  $t$ , the interferor strength is reduced by a factor  $\text{sinc}(\nu_f t)$  relative to the desired

---

<sup>1</sup>For an offset equal to the antenna beamwidth,  $\theta \sim \lambda/D$ , it is easy to show that the maximum differential signal (‘fringe’) frequency is  $\nu_m = \omega_e B/D$ , where  $B$  is the interferometer baseline and  $D$  is the antenna diameter. For the VLA in ‘A’ configuration this differential fringe frequency is 0.10 Hz. An integration time not exceeding  $\sim 1$  second is thus required to retain the coherence for emission throughout the primary beam.

signal, where  $\text{sinc } x = (\sin \pi x)/\pi x$ . For large values of  $x$ , the attenuation becomes  $1/\nu_f t = 1/(\text{Number of turns of phase})$ . Thus, if one has the luxury of integrating over very long times (which means in effect that the field of view is vanishingly small), the interferometer's natural fringe winding will reduce the interfering signal by a factor given by

$$A \sim \frac{\lambda}{\omega_e t B \cos \delta} \quad (7)$$

This attenuation can be very large for long-baseline, short-wavelength interferometers – a factor exceeding a million for an hour-long, 35-km baseline observation at 7mm of an equatorial source. This attenuation could be considerably improved, if a more sophisticated averaging function were employed.

Although this analysis is useful for indicating how the interfering signal is attenuated by a phase-tracking interferometer, it is not applicable to an imaging array, where the integration time is limited by the size of the object under study, and the imaging is necessarily two-dimensional. In the next section, these complicating effects are taken into account.

## 4 RFI from an Imaging Perspective

Consider a short burst of interference, where short is defined as a time duration much less than the fringe period:  $t \ll \lambda/\omega_e B \cos \delta$ . The correlator will produce a complex number for each baseline, describing the amplitude and phase of the RFI, as modulated by the sidelobe(s) through which it enters. The imaging process places on the image plane, for each measured visibility, a two-dimensional sinusoid with an amplitude given by the visibility amplitude, an offset with respect to the phase tracking center given by the visibility phase, and an orientation determined by the (u,v) coordinates of the baseline as seen by the phase tracking center at the time of the observation. The resulting ‘image’ of the RFI is the sum of all the sinusoids.

For an image of the target object, the phases of the emission are coherent (after calibration) at the map locations corresponding to the true source emission, so the sums of all the sinusoids at this location reflect the true brightness of the object of interest. But at other locations, for other objects, including unwanted emissions entering through sidelobes, the averaging process can be considered as incoherent.

The rms in the image due to the RFI on a single baseline is simply  $S_0/\sqrt{2}$ , where  $S_0$  is the amplitude of the RFI signal. Now assume for simplicity that the sidelobe gain of all antennas is the same and constant. Then the rms in the image due to  $N_b$  interferometers will be  $S_0/\sqrt{2N_b}$ . If the number of antennas in the array,  $N$ , is large, and all pairs are correlated, then  $N_b = N(N-1)/2$ , and we get for the rms in the image,  $\sigma \sim S_0/N$ .

Although we have argued that the image of the RFI is incoherent because of the varying phase of the sidelobes and propagation path, the calculation of the rms is independent of the phase properties of the correlated signal. This is in fact a manifestation of Rayleigh's theorem in Fourier transform theory. Stated another way – even if the pulse of interference was coherent in the sense that it came from a direction in the field of view, and the phases were calibrated so that the image showed the full amplitude of the pulse, the rms in the entire image would remain the same. The phases of the emission affect the structural details of the emission, but do not affect the rms. Thus, the effect on an image due to a short-duration pulse of unwanted emission is attenuated by a factor of  $\sim 1/27$ , or  $-14$  dB compared to a total-power system.

In Figure 1, we show the effect on an image made at a declination of 80 degrees due to a short duration pulse of unit amplitude. In the left panel, the phases of the pulse are appropriate for a ‘real’ source at the north pole. In the right panel, the phases of the data have been randomized to simulate the effect of a pulse entering through the sidelobes. Although the details of the responses are different, the rms of each is the same.

We now consider the effect on an image when observing the RFI over a period of time much longer than the natural fringe period,  $t > \lambda/\omega_e B \cos \delta$ . This image can be considered as the average of a large number of sequential snapshots, each separated by a time short compared to the fringe period. Each contributing snapshot image has the appearance of Figure 1, but as time goes on, the sidelobes move in accordance to the changing geometry of the array and the changing peculiar phases of each antenna. For the case of a ‘real’ source at the north pole, the changing pattern is simply a rotation of the sidelobes emanating from the object. For the case of an ‘incoherent’ object, the same process occurs, but the ‘sidelobes’ are changing their distribution on a timescale given by the timescale of phase changes of the received signal. Generally, the shorter timescale is that of the fringe rotation, so we can consider as independent those snapshot images separated by a time given by the fringe period of the longest baseline. As the resultant image is the average of the input snapshots, we expect the rms in this image to decline as  $1/\sqrt{N_s}$ , where  $N_s \sim t\omega_e B \cos \delta/\lambda$  is the number of independent observations within the observing time,  $t$ . The same result can be obtained by noting that the angular rotation rate of the sidelobes

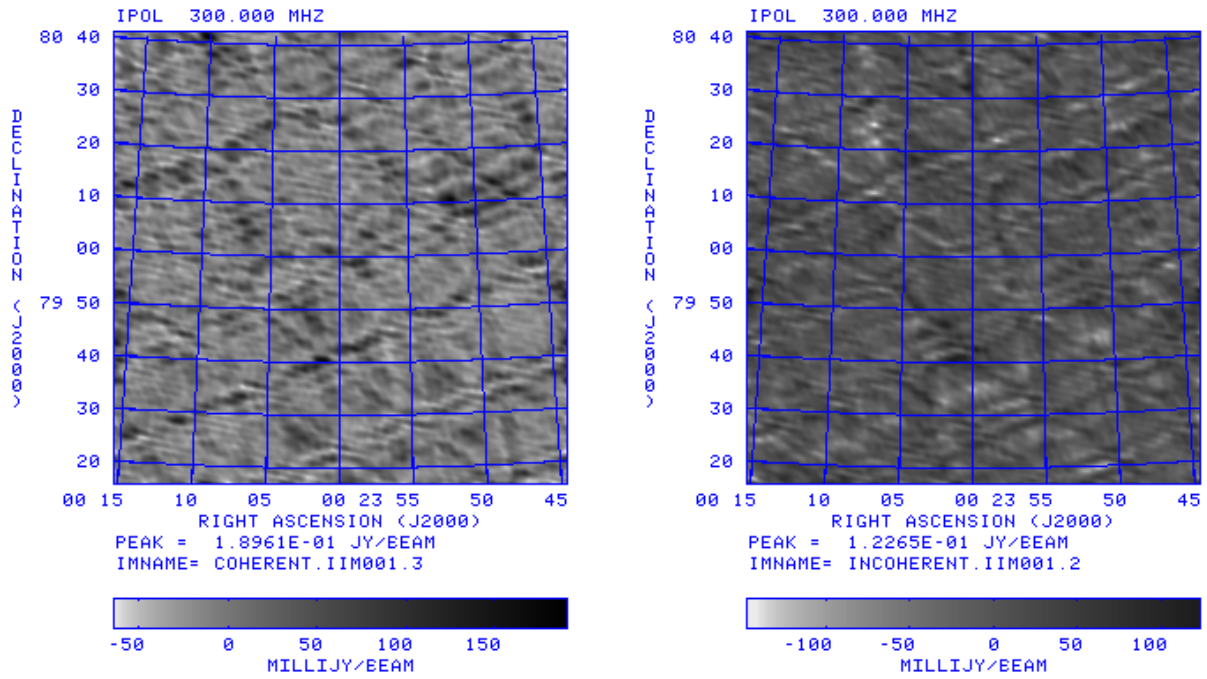


Figure 1: Showing the effect on a snapshot image for  $\delta = 80$  of a source of 1 Jy. In the left panel, the phases are appropriate for an object at the north celestial pole. In the right panel, the phases have been randomly adjusted, to simulate the effects of far sidelobes. The rms in the left panel is 0.027 Jy, in the right panel 0.025 Jy. The effective attenuation is  $-16$  dB, compared to the predicted  $-14$  dB of a simple analysis.

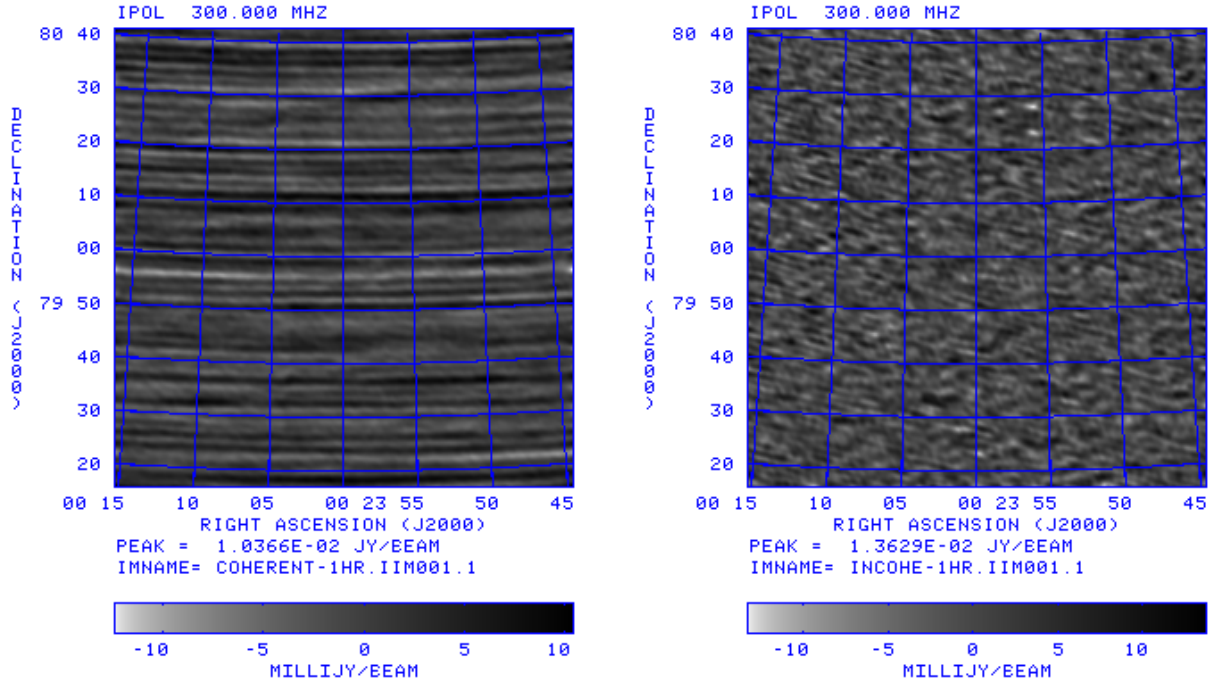


Figure 2: Showing the effect on a 1-hour integration for  $\delta = 80$  of a source of 1 Jy. In the left panel, the phases are appropriate for an object at the north celestial pole. In the right panel, the phases have been randomly changed every minute, to simulate the effects of far sidelobes or propagation path differences. The left image shows the 'streaks' caused by rotation of the north polar dirty beam corresponding to the 1 Jy image. In the right image, these streaks are absent since the random phase changes are occurring on a much shorter timescale than the image rotation. The rms in both panels is 0.0030 Jy. The effective attenuation is  $-25.2$  dB, compared to the predicted  $-27$  dB of a simple analysis, using a baseline length of half the maximum.

in a map is  $\omega = \omega_e$ , so at a distance of  $q = \cos \delta$ , in time  $t$ , the distance travelled in the image is  $\omega_e t \cos \delta$ . As the typical sidelobe scale in the image is  $\theta \sim \lambda/B$ , (where  $B$  is some median distance, to be defined later), the number of sidelobes passing any point in time  $t$  is  $N_s \sim \omega_e t B q / \lambda$ . As the height of each sidelobe is  $\sim S_0/N_a$ , the expected rms in the images becomes

$$I \sim \frac{S_0}{N_a \sqrt{N_s}} = \frac{S_0}{N_a} \sqrt{\frac{\lambda}{\omega_e t B q}} \quad (8)$$

Figure 2 shows the imaging effects for a one-hour integration at declination of 80 degrees, with a 1 Jy source placed at the north pole. As before, the left panel shows the result for a phase coherent object (a 'real' source), while the right panel shows the result when the phases randomly change once every minute. The rms is the same in each, 0.003 Jy, corresponding to  $-25.3$  dB attenuation.

In this analysis, the interpretation of the baseline  $B$  is left undefined. It must clearly depend on the distribution and weighting of baselines in the transform (u,v) plane, and hence on the integration time and the distribution of antennas within the array. In the Appendix is presented an alternate analysis, which results in a definition of the effective baseline,

$$B_m = \left( \frac{1}{N_b} \sum_{i=1}^{N_b} \frac{1}{B_i} \right)^{-1} \quad (9)$$

and gives scaling coefficient of  $1/\sqrt{\pi}$ , resulting in a predicted attenuation of

$$R(t) \sim \frac{1}{\sqrt{\pi} N_a} \sqrt{\frac{\lambda}{\omega_e t B_m q}} \quad (10)$$

We compare this result to that derived by Thompson[2], as reproduced in Thompson, Moran and Swenson[3]. Thompson’s approach is to calculate the attenuation of the signal within a given cell in the gridded (u,v) plane, then sum over all occupied cells within that plane. The fringe-winding attenuation from his approach can be obtained by dividing equation 15.2 by 15.12, to give

$$R_T = \sqrt{\frac{\lambda}{2\omega_e t q \frac{1}{n_r} \sum_{n_r} B}} \quad (11)$$

where the sum is over all cells in the gridded u-v plane. The angular dependence  $q$  in their analysis is slightly different:  $q = \cos \delta(1 + |\sin \delta|)$ .

Both approaches give identical dependencies – that the attenuation of a stationary interfering signal by fringe rotation is proportional to the inverse square root of the product of: (a) the earth’s rotation rate, (b) the duration of the interference, (c) the frequency, (d) the array scale, and (e) the sine of the angular distance from the north pole (with an additional, smaller term in the treatment of Thompson). The differences come from the differing treatments of the distribution of the measured visibilities in the u,v measurement plane. Both treatments define a ‘mean baseline’ which is dependent upon the number and distribution of points in the transform plane. This mean baseline is difficult to define in general, as it depends upon many array and observational parameters.

## 5 Simulations

The preceding expressions give useful insight into the mechanism of how an imaging interferometer reduces the effects of unwanted external signals. To check the predicted dependencies of the attenuation on declination, averaging time, frequency and baseline, it is easiest to simulate the effects using existing imaging software. This has been done using the AIPS package, using the following methodology:

- A ‘blank’ database was generated using the program UVCON, for a specific declination, frequency, array configuration, and hour angle range. The sampling time was carefully adjusted to obtain at least 40 samples per fringe period for a source at the north celestial pole. Such fine sampling is necessary to ensure that the full effects of the vector cancellation are retained. (It also results in extremely large databases, which necessarily restricted the simulations to low frequencies or short configurations.
- The visibilities for a source located at the north celestial pole were added using UVMOD.
- An image of the source at the north pole, and of its sidelobes at the declination of interest were created using IMAGR.

A wide range of simulations was generated, covering all four configurations, hour angle coverages (or RFI durations) between 2 seconds and 24 hours, frequencies between 300 MHz and 5 GHz, and declinations between  $-40$  and  $90$  degrees. Examples of the generated images are shown in Figure 3, for an equatorial object observed for ten hours, and in Figure 4, for a source at a declination of  $80$  degrees observed for 12 hours. In each figure, the left panel shows the image, while the right panel shows the amplitudes in the transform (u,v) plane. Although these simulations were made using a ‘coherent’ source, there is no change in the results for an ‘incoherent’ object, whose phases are modulated by sidelobes or propagation effects.

In Figure 3, the imaging effects from the stationary source (left panel) are nearly perfectly horizontal. From the point of view of imaging, this pattern occurs because of the rotation of the snapshot pattern about the north pole. The right panel shows the residual signal in the (u,v) plane. The only notable visibilities are distributed along the  $u = 0$  axis, where the fringe rate is zero. The reason for the vertical symmetry is that the motion of the baselines is a function of  $u$  only – it is independent of  $v$ . Since the fringe rate is also only a function of  $u$ , the phase rotation within any (u,v) cell and hence the resulting attenuation in that cell, is therefore independent of  $v$ .

Figure 4 shows the residual RFI, and the visibility signal, at a target declination of  $80$  degrees. The left panel shows that the image effects follow lines of constant declination, which are again due to the rotation of an unchanging snapshot pattern about the north pole. In the signal plane (right panel), the significant visibilities are seen to be spread out in a cone centered on the  $v$  axis, with vertex at the origin. The explanation for this effect is of some interest. The attenuation in any given cell in the (u,v) plane is dependent upon the total phase rotation within that cell. This, in turn, is proportional to the phase rate of the baseline multiplied by the time

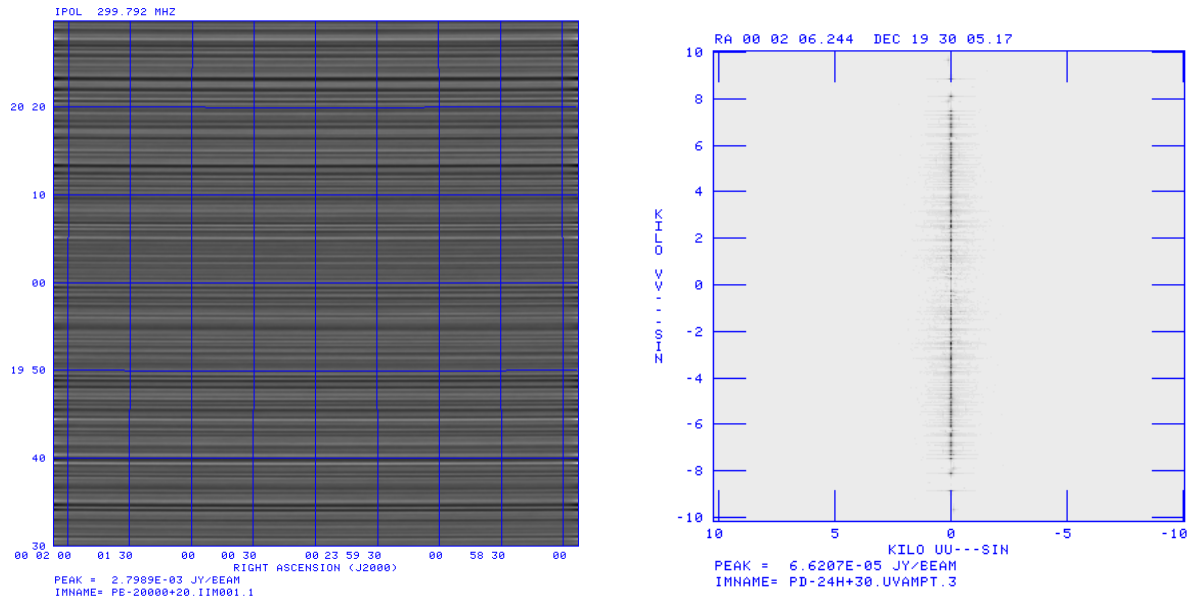


Figure 3: Showing the image sidelobes (left panel) and  $u,v$  amplitudes for an observation at declination = 0, for a source located at the north celestial pole. The attenuation is high everywhere except along the  $u = 0$  axis, where the phase rate is zero. The right panel shows the amplitudes of the visibilities in the  $(u,v)$  plane.

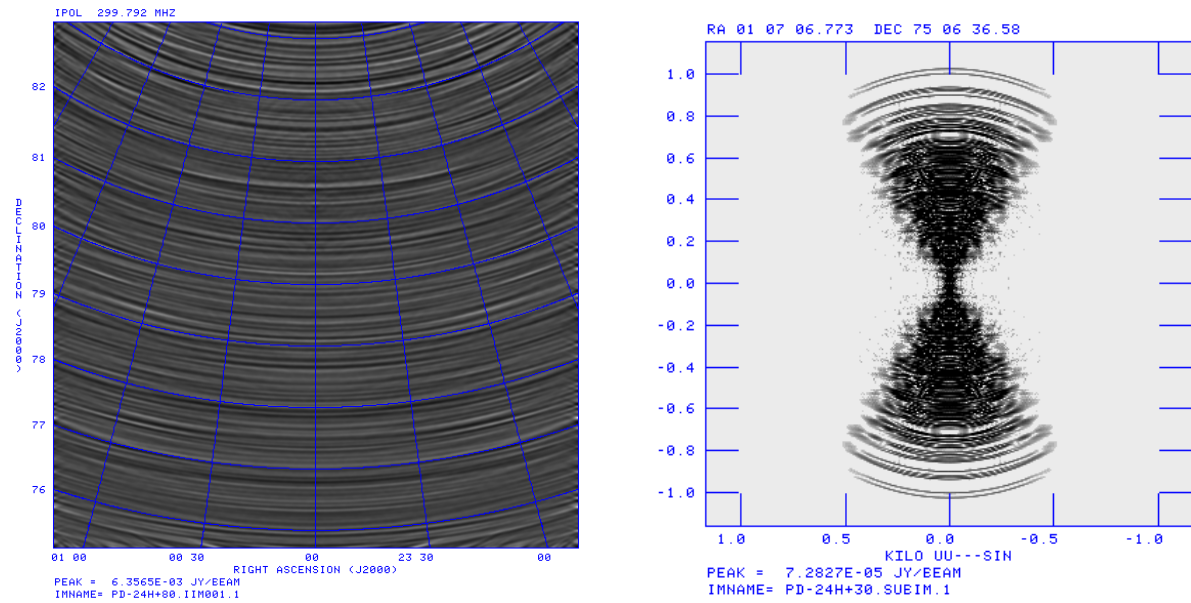


Figure 4: Showing the image disturbance (left panel) and  $u,v$  amplitudes (right panel) at a declination of 80 degrees, for a source located at the north pole. The attenuation in any given cell is dependent upon the ratio of the phase rate – a function only of  $u$ , to the velocity of the baseline while traversing that cell. The attenuation is low in a sector (right panel) at this high declination because the long baselines move quickly, and are located only in the outer regions of the  $(u,v)$  plane, and the phase rate depends on  $\cos \delta$ .

is takes that baseline to traverse that cell, which in turn is inversely proportional to the motion of the baseline in the (u,v) plane. The total phase rotation within a cell can then be expressed as:

$$\Delta\phi \propto \frac{\omega_e u \cos \delta}{\sqrt{(du/dt)^2 + (dv/dt)^2}} \quad (12)$$

which can be expressed as

$$\Delta\phi \propto \frac{\omega_e u \cos \delta}{\sqrt{u^2 \sin^2 \delta + \left(\frac{v - B_z \cos \delta}{\sin \delta}\right)^2}} \quad (13)$$

where  $B_z$  is the component of the baseline parallel to the Earth's rotation axis. For declinations near 90 degrees, this expression can be simplified to

$$\phi \propto \frac{\omega_e u \cos \delta}{\sqrt{u^2 + v^2}} \rightarrow \omega_e \Delta\delta(u/r) \quad (14)$$

where  $r$  is the radial distance in the (u,v) plane from the origin, and  $\Delta\delta = 90 - \delta$ . This result shows that the lines of constant attenuation for northern objects radiate at constant angle from the origin, as shown in Figure 2, right. The attenuation within a cell is small, despite the long baselines, because these baselines travel so rapidly through the (u,v) plane, in a region where the fringe period is longer (due to the northern declination and because the coordinate value  $u$  is small).

The dependencies of the rms sidelobe patterns on averaging time, maximum baseline length, frequency, and target source declination, are shown in Figure 5. For each panel, selected trial results are plotted, showing in each the expected slope of 5 dB/decade.

Equation 10, which gives the expected attenuation, can be expressed in more practical units as follows

$$R = \frac{1.34}{\sqrt{t_s \nu_M B_K \cos \delta}} \quad (15)$$

where  $t_s$  is the duration of the RFI in seconds,  $\nu_M$  is the frequency in MHz, and  $B_K$  is the mean baseline in kilometers. For a given array, this mean distance will be approximately linearly related to the maximum baseline. Define  $f$  as the ratio between the maximum baseline and the mean baseline of the array:  $f = B_{max}/B_m$ , giving for our final expression for the attenuation of an interfering signal by the imaging process

$$R = \frac{1.34\sqrt{f}}{\sqrt{t_s \nu_M B_{max,K} \cos \delta}} \quad (16)$$

The VLA's compacted geometry would suggest that the ratio of the maximum to mean baseline is approximately four, suggesting that the actual coefficient in the preceding equation will be about 2.6.

We show in Figure 6 a comparison of the estimated attenuation, taken from Equation 16, using a numerator of 2.6, to that measured from the simulations. The agreement is generally very good, with the exception of those observations where the predicted attenuation is low, and where the actual attenuation asymptotes at about 14 dB. This flattening in attenuation is because the duration of the observation is insufficient for any significant fringe winding, so that the only attenuation available is that due to the 351 VLA baselines adding incoherently. The transition between these two dependencies occurs when

$$t_s \nu_M B_{max,K} \cos \delta \sim 4260 \quad (17)$$

where we remind the reader that  $B_{max,K}$  is the maximum baseline in the array, measured in kilometers.

## 6 Discussion

The results of the simulations show that Equation 16 is remarkably accurate in predicting the attenuation of a constant amplitude external signal due to the phase rotation of a tracking interferometer. For the extreme case of a 12-hour interfering signal, observed at 49 GHz with the VLA in its A-configuration, the attenuation will be  $\sim -50$  dB! In more practical cases, attenuations of  $-20$  to  $-30$  dB can be expected. In all cases, attenuation of  $-14$  dB is obtained simply from the incoherent summation over the array's baselines.

These results can be extended to non-stationary interference by the following argument. In essence, the attenuation is inversely proportional to the total number of fringes traversed by the target source in the given



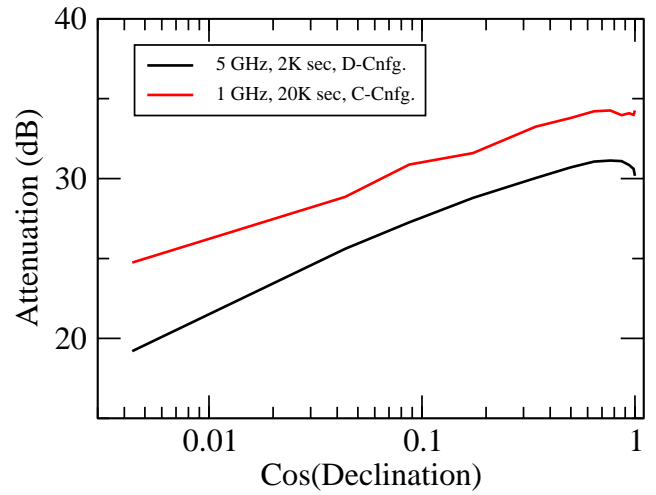
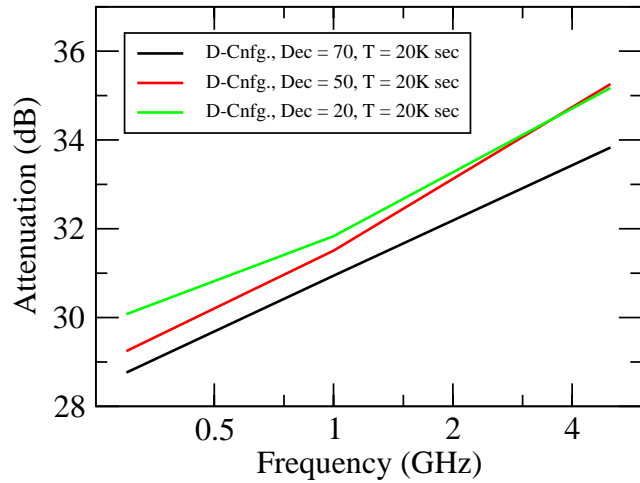
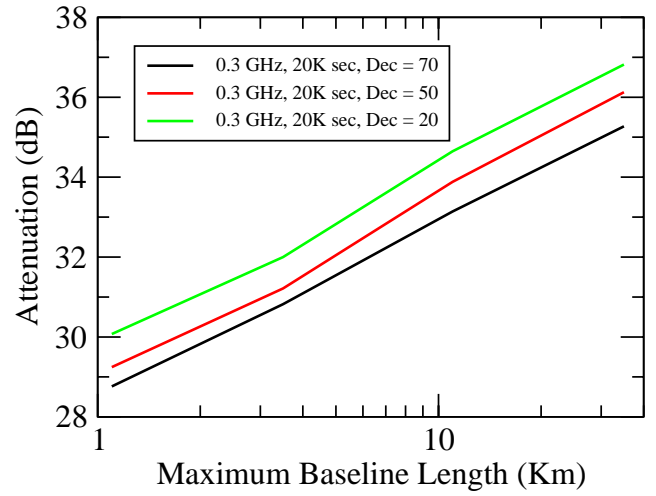
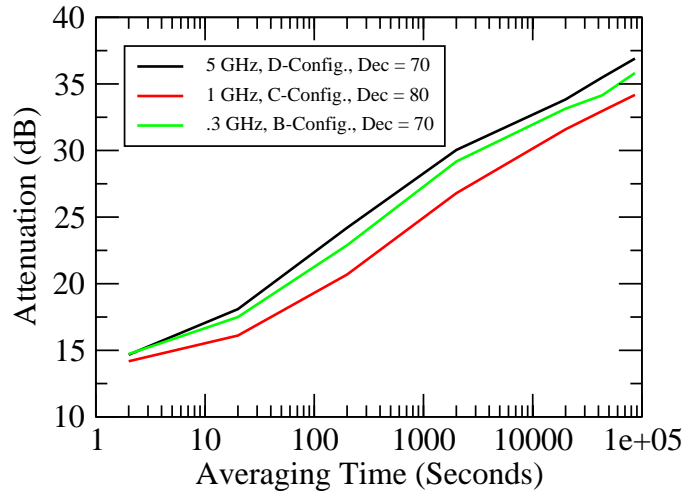


Figure 5: Simulations showing the rms sidelobe level for stationary RFI for different configurations, frequencies, time averaging and declinations.

# Interferometric Attenuation of Stationary Signals

## Comparison of Prediction with Simulations

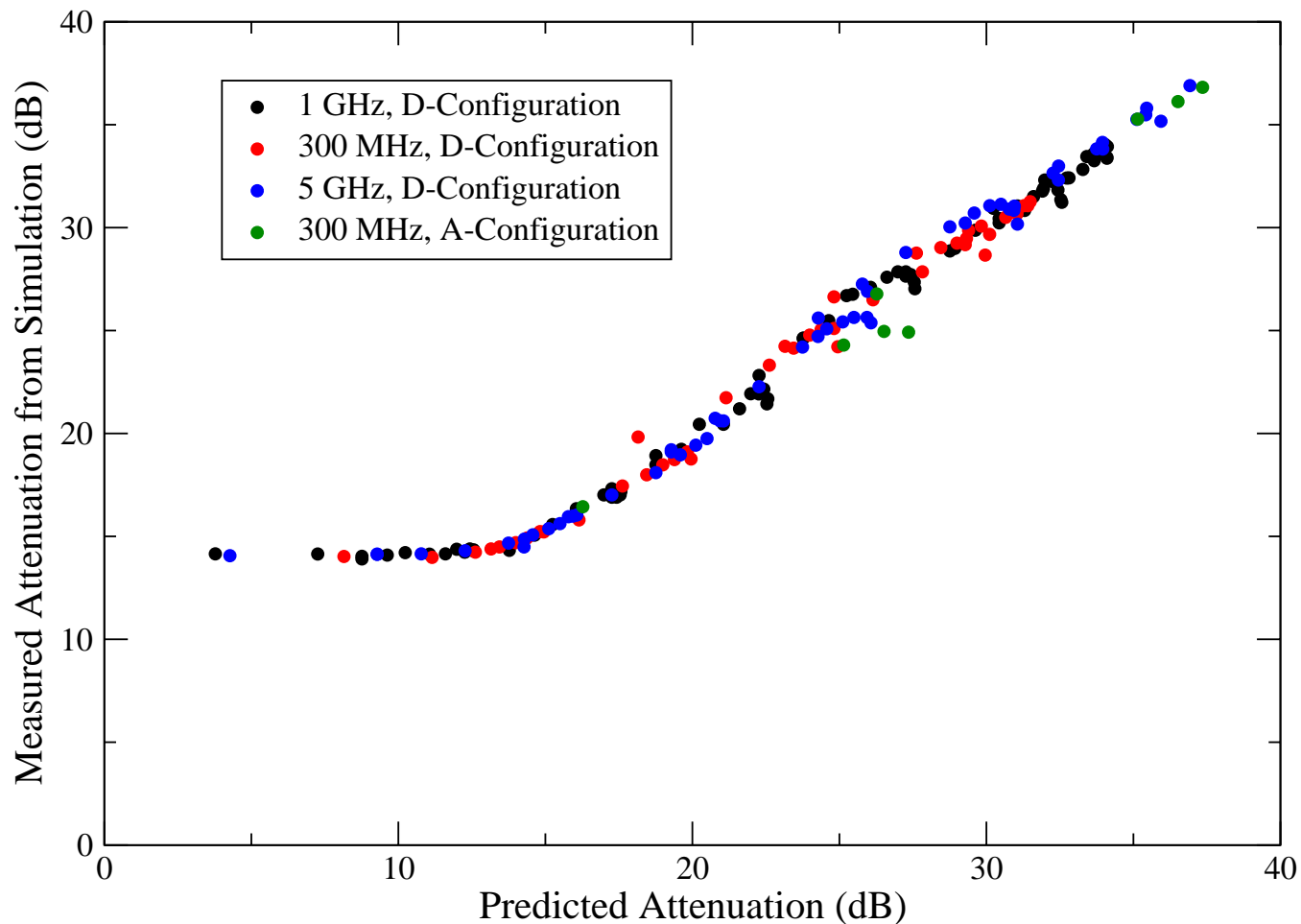


Figure 6: A comparison of the predicted attenuation, using Equation 16 with  $f = 4$ , to that measured in simulations, for a range of target declinations, integrations, frequencies, and array configurations.

observation time. If, in a period of time  $t$ , a moving source of interference traverses  $N$  fringes, we would expect an attenuation of order  $1/\sqrt{N}$ . A moving interferor, travelling at an angular rate  $\omega$  for time  $t$  will pass  $\sim B\omega t/\lambda = Bvt/\lambda r$  fringes, where  $v$  is the velocity, and  $r$  the distance of the interferor. And we would expect the attenuation to be even stronger in the case where the angular movement of the interferor is much greater than that of the astronomical source, since in that situation the coherent addition will lie within one, or only a few, (u,v) cells. In this case, the analysis of Section 3 will apply, so the effect in the image will decline with  $1/N$ , rather than  $1/\sqrt{N}$  (and potentially even better, with more sophisticated averaging schemes).

This analysis shows that for the VLA and EVLA, the tolerance of the array to an interfering source of emission is significantly higher than for an equivalent total power system. Besides the obvious benefit of this for diminution of unwanted external emissions, this improved isolation will enable a significant relaxation of the stringent emission standards for equipment located at the VLA site. At a minimum, the allowed emissions can be higher by  $\sim 15$  dB than those indicated by application of equation 3.

## A An Alternate Analysis of the Fringe-Winding Attenuation

From the perspective of the correlator, RFI from a stationary source is indistinguishable from emission from a source located in the direction of the north celestial pole, as both have a zero natural fringe rate, other than the slow modulation added by the antennas' gain variations, and by propagation path differences. We use this fact to estimate the effects of such a source on the image at an arbitrary declination and hour angle.

Consider an astronomical observation in the direction of the north celestial pole, during which an interfering signal enters the array antennas through the sidelobes. In a 12-hour observation, the locus of each baseline describes a half-circle in the u-v plane, of radius  $B/\lambda$ . To simplify the problem, we assume for now that the antennas' sidelobe gains are unchanging, and that their phases are the same, so that the correlator phase is zero, and the amplitude constant with apparent spectral flux density  $S_0$ . Then, the imaged response to the interference from a single baseline will be given by a Bessel function of order zero:

$$I(q) = S_0 J_0 \left( 2\pi \frac{B}{\lambda} q \right) \quad (18)$$

where  $B$  is the baseline length, and  $q$  is the sine of the angle from the north pole (the map center):  $q = \cos \delta$ .

We are interested in the sidelobe response from this 'source' at great distance. The asymptotic approximation for the  $J_0$  Bessel function at large angle,  $q \gg \lambda/B$  is

$$I(q) \rightarrow \frac{S_0}{\pi} \sqrt{\frac{\lambda}{Bq}} \cos \left( 2\pi \frac{B}{\lambda} q - \frac{\pi}{4} \right). \quad (19)$$

Each baseline contributes a zero mean, oscillating contribution whose amplitude declines as the square root of distance from the north pole. The root-mean-square in these sidelobes is then

$$I_{rms}(q) = \frac{S_0}{\sqrt{2\pi}} \sqrt{\frac{1}{Bq}} \quad (20)$$

As each baseline is of different length, and assuming that each contributes equally to the output (uniform weighting), the summed response over many baselines, relative to the image's peak response, declines with the square root of the number of baselines, or linearly with the number of antennas. We thus find, for the rms far-field disturbance, after summing over all baselines and normalizing by the peak response,

$$R \sim \frac{1}{\sqrt{2\pi}} \sqrt{\frac{\lambda}{N_b B_m q}} \rightarrow \frac{1}{N_a \pi} \sqrt{\frac{\lambda}{q B_m}} \quad (21)$$

where  $N_a$  is the number of antennas in the array,  $N_b = N_a(N_a - 1)/2$  is the number of baselines, and the 'mean' baseline  $B_m$  is an average over all  $N_b$  baselines:

$$B_m = \left( \frac{1}{N_b} \sum_{i=1}^{N_b} \frac{1}{B_i} \right)^{-1}. \quad (22)$$

$R$  in Eqn. 20 is interpreted as the effective attenuation due to the imaging process.

This analysis assumes the signal is on for twelve hours – long enough for the baseline locus (plus its complex conjugate) to complete a circle in the  $u$ - $v$  plane. For shorter times, we note that the angle traveled by the locus of the baseline is given by  $\phi = \omega_e t$ , where  $\omega_e$  is the angular rotation rate of the earth. This suggests that for shorter times, the appropriate expression for the response at great distance is

$$R(t) \sim \frac{1}{\sqrt{\pi}N_a} \sqrt{\frac{\lambda}{\omega_e t B_m q}}. \quad (23)$$

This rough estimate can be justified by noting that  $\omega_e t B q / \lambda$  is the number of spatial cycles of the interferometer fringe which sweep through the north pole in time  $t$  when observing a source at declination  $\delta$ . We also can anticipate that this attenuation due to the rotation of the earth will not be effective when the number of fringes passed is small.

## References

- [1] Rick Perley. *RFI Emission Goals for EVLA Electronics*. EVLA Memo Series, #46, October 2002.
- [2] A. Richard Thompson. *The Response of a Radio-Astronomy Synthesis Array to Interfering Signals*. IEEE Transactions on Antennas and Propagation, Vol. AP-30, No. 3, May 1982, pp. 450 – 456.
- [3] A. Richard Thompson, James M. Moran, George W. Swenson, Jr. *Interferometry and Synthesis in Radio Astronomy, 2nd Edition*, John Wiley & Sons, Inc. 2001.